

# Collimated Ultra-Bright Gamma-Rays from a PW-Laser-Driven Wire Wiggler

W.-M. Wang,<sup>1,2</sup> Z.-M. Sheng,<sup>3,4,5,6</sup> P. Gibbon,<sup>7,8</sup>  
L.-M. Chen,<sup>1,5</sup> Y.-T. Li,<sup>1,5,9</sup> and J. Zhang<sup>4,5</sup>

<sup>1</sup>*Beijing National Laboratory for Condensed Matter Physics,  
Institute of Physics, CAS, Beijing 100190, China*

<sup>2</sup>*Beijing Advanced Innovation Center for Imaging Technology  
and Key Laboratory of Terahertz Optoelectronics (MoE),  
Department of Physics, Capital Normal University, Beijing 100048, China*

<sup>3</sup>*SUPA, Department of Physics, University of Strathclyde,  
Glasgow G4 0NG, United Kingdom*

<sup>4</sup>*Key Laboratory for Laser Plasmas (MoE) and School of Physics and Astronomy,  
Shanghai Jiao Tong University, Shanghai 200240, China*

<sup>5</sup>*IFSA Collaborative Innovation Center,  
Shanghai Jiao Tong University, Shanghai 200240, China*

<sup>6</sup>*Tsung-Dao Lee Institute, Shanghai Jiao Tong University, Shanghai 200240, China*

<sup>7</sup>*Forschungszentrum Jülich GmbH, Institute for Advanced Simulation,  
Jülich Supercomputing Centre, D-52425 Jülich, Germany*

<sup>8</sup>*Centre for Mathematical Plasma Astrophysics,  
Katholieke Universiteit Leuven, 3000 Leuven, Belgium*

<sup>9</sup>*School of Physical Sciences, University of Chinese  
Academy of Sciences, Beijing 100049, China*

(Dated: July 5, 2021)

## Abstract

It is shown by three-dimensional QED particle-in-cell simulation that as a laser pulse of 2.5 PW and 20 fs propagates along a sub-wavelength-wide solid wire, directional synchrotron  $\gamma$ -rays along the wire surface can be efficiently generated. With 8% energy conversion from the pulse, the  $\gamma$ -rays contains  $10^{12}$  photons between 5 and 500 MeV within 10 fs duration, corresponding to peak brilliance of  $10^{27}$  photons  $\text{s}^{-1}$   $\text{mrad}^{-2}$   $\text{mm}^{-2}$  per 0.1% bandwidth. The brilliance and photon energy are respectively 2 and 3 orders of magnitude higher than the highest values of synchrotron radiation facilities. The radiation is attributed to the generation of nC, GeV electron beams well guided along the wire surface and their wiggling motion in strong electrostatic and magnetostatic fields induced at the high-density-wire surface. In particular, these quasistatic fields are so strong that QED effects already play a significant role for the  $\gamma$ -ray radiation. With the laser power  $P_0$  ranging from 0.5 PW to 5 PW available currently, this scheme can robustly produce  $\gamma$ -rays peaked at  $1^\circ$  with few-mrad divergence and the photon energy and number roughly scales with  $P_0$  and  $P_0^{3/2}$ , respectively. Our scheme embraces both the merits of high directionality comparable to those based upon laser wakefield acceleration and high charge comparable to those based upon laser-solid interaction.

PACS numbers: 52.38.Ph, 52.38.-r, 52.59.Px, 41.75.Fr, 52.65.Rr

Bright  $\gamma$ -rays with energy above MeV are highly demanded in broad applications ranging from laboratory astrophysics [1], emerging nuclear photonics [2, 3], to radiotherapy [4, 5]. These applications can potentially benefit from  $\gamma$ -ray sources based upon compact laser-driven electron acceleration. Via laser wakefield acceleration (LWFA) [6, 7], GeV electron beams typically with duration of tens of fs, transverse size of micrometers, and divergence of a few mrad are generated from gas plasma. Through betatron radiation [8–10] or Compton scattering [11–18] the beams are wiggled by electrostatic or/and laser fields and then emit  $\gamma$ -rays basically with similar duration, size, divergence to the beams. These cause high peak brilliance  $10^{19} - 10^{23}$  photons  $s^{-1}$  mrad $^{-2}$  mm $^{-2}$  per 0.1% bandwidth (BW). Mainly limited by wiggler field strengths, most  $\gamma$ -ray photons are distributed in sub-MeV range. By increasing the scattering laser strength [15, 18] or frequency [14], the Compton photon energy can be enhanced to multi-MeV. However, both the energy conversion efficiency from the pulse to the  $\gamma$ -rays and the resulting photon number are not high, typically around  $10^{-6}$  [12] and  $10^6 - 10^8$  photons [9, 10, 13, 15], respectively, due to limited charge in LWFA beams and wiggler strengths.

To overcome these limits and further enhance the photon energy to the GeV range, we propose a scheme in which a currently-available PW laser pulse [19–21] propagates along a sub-wavelength wire, as shown in Figs. 1(a) and 1(b) (three-dimensional direct laser writing [22] can provide wire arrays). Making use of the high density of the wire, a directional GeV electron beam with tens of nC charge is generated along its surface. Meanwhile, electrostatic and magnetostatic fields induced at the surface are strong, which intensively wiggles the beam electrons with significant QED parameters. By QED synchrotron radiation from the GeV nC beam, 8% laser energy ( $10^5$  higher than those based upon LWFA) is converted to directional  $\gamma$ -rays containing  $10^{12}$  photons with energy up to GeV according to our 3D particle-in-cell (PIC) simulations. The  $\gamma$ -rays, inheriting the laser duration and wire width, have a high brilliance second only to X-ray free electron lasers (XFEL), while the average photon energy of 20MeV is 3 orders of magnitude higher than XFEL, as shown in Fig. 1(f) and Refs. [23–26].

We show for the first time that the PW-laser-irradiated sub-wavelength wire acts as a novel wiggler as well as an accelerator of collimated electron beams of nC. Note that the wire accelerator has been widely studied [27–31]. Here, we show wiggling of the beam electrons due to the electrostatic and magnetostatic fields induced around the high-density

wire surface, which are so high that QED effects become significant. This is different from nonlinear Compton scattering [32–34] or resonance acceleration [35] in the QED regime, which is driven directly by laser fields with powers above 10PW. Besides, in a previous channel-like-target scheme [36], the wiggling electrons are across the whole channel with the transverse size near the laser spot diameter and therefore the generated photons have emission angles of  $40^\circ$ . In our scheme the wiggling electrons are restricted around the wire surface, which causes the photons peaked at  $1^\circ$  with few-mrad divergence. To our knowledge, our scheme produces the  $\gamma$ -ray emission with the best directivity so far based on laser-solid interaction.

We demonstrate our scheme [see Fig. 1(a)] through 3D PIC simulations with the KLAPS code [37] including photon and pair generation via QED processes [34, 38]. The pulse propagates along the  $+x$  direction with  $y$ -direction polarization, wavelength  $1\mu\text{m}$  (period  $\tau_0 = 3.3\text{fs}$ ), peak power 2.5PW, and FWHM duration 20fs. With an initial spot radius  $r_{ini} = 6.12\mu\text{m}$  and amplitude  $a_{ini} = 56$  normalized by  $m_e c \omega_0 / e$  (intensity  $4.3 \times 10^{21} \text{ Wcm}^{-2}$ ), the pulse is located at 5 Rayleigh lengths ( $22.6\mu\text{m}$ ) ahead of the focusing plane. The spot radius at the focusing plane are expected to be  $r_0 = 1.2\mu\text{m}$  with  $a_0 = 285$  in the vacuum. An aluminium wire of cuboid is taken with  $50\mu\text{m}$  long in the  $x$  direction and  $0.6\mu\text{m}$  wide, which is placed  $2.4\mu\text{m}$  behind the pulse initial wavefront. It is assumed as fully-ionized plasma of density  $690n_c$  ( $n_c = 1.1 \times 10^{21} \text{ cm}^{-3}$ ) with a  $0.2\mu\text{m}$ -exponential-scalelength preplasma. A moving window at the light speed is taken with a simulation box  $16\mu\text{m} \times 24\mu\text{m} \times 24\mu\text{m}$  in  $x \times y \times z$  directions. We take the cell sizes in the three directions as  $0.02\mu\text{m}$ , the timestep as 0.033fs (adjustable timesteps for photon and pair generation [34]), and 8 quasi-particles per cell.

Figures 1(c)-1(e) show the  $\gamma$ -rays emitted from the wire as well as from a flat aluminium target with a large enough transverse size of  $24\mu\text{m}$  for comparison. With the wire, the  $\gamma$ -rays have a sharp peak angle nearly along the wire surface [see Fig. 1(d)]. However, large divergence  $\gamma$ -rays are generated with the flat target, as obtained in previous reports [32, 33]. Although the energy conversion efficiencies are similar in the two cases, the photon number in the peak angle is one order of magnitude higher in the wire case. Figure 1(c) shows that the  $\gamma$ -rays have FWHM duration about 10fs and a transverse size near the wire width  $0.6\mu\text{m}$  because they are generated around the wire surface. **The brilliance is  $1.2 \times 10^{27}$ ,  $8 \times 10^{26}$ , and  $1.5 \times 10^{26}$  photons  $\text{s}^{-1} \text{ mrad}^{-2} \text{ mm}^{-2}$  0.1% BW at 5MeV, 20MeV, and**

100MeV, respectively, where the total  $\gamma$ -rays have  $1.75 \times 10^{10}$  photons in the angle  $1^\circ$  with the divergence of  $3.49 \times 3.49$  mrad<sup>2</sup> (we count the photon number with an angle displacement of  $0.2^\circ$ ). With the flat target, the source size is increased to a few microns, determined by the plasma area of laser hole boring [39]. The increased size and decreased photon number at the peak angle causes the peak brilliance reduced by 3 orders of magnitude. Figure 1(e) shows the photon spectrum distributed from 5MeV to 500MeV with average energy about 20MeV in the wire case. Note that some beam electrons with energy above 1GeV which can emit photons of 500MeV since the electron QED parameters [40–42]  $\chi > 0.2$  [see Fig. 3]. With the flat target, both the photon energy and the number in the higher-energy part are significantly reduced. This suggests that the wire geometry is more favorable to bring larger  $\chi$  for higher photon energy.

We examine the wiggler fields in detail. The fields composed of electrostatic and magnetostatic components are perpendicular to velocities of the beam electrons moving along the  $+x$  direction. First, the laser field strips a large number of electrons away from the wire surface [see Fig. 2(b)], which induces electrostatic fields  $E_y^S$  [see Fig. 2(a)] and  $E_z^S$  around the surfaces  $y \simeq \pm 0.3\mu m$  and  $z \simeq \pm 0.3\mu m$ , respectively. In turn, the laser field becomes hollow as observed in Fig. 1(b). Due to radiation pressure, the hollow laser pulse together with the electrostatic fields tends to confine electrons within the wire. To compensate the beam-electron flux along the  $+x$  direction, a return current is formed around the wire surface [see Fig. 2(d)], which induces magnetostatic fields  $B_z^S$  [see Fig. 2(c)] around  $y \simeq \pm 0.3\mu m$  and  $B_y^S$  around  $z \simeq \pm 0.3\mu m$ . According to Figs. 2(a) and 2(c),  $E_y^S$  and  $B_z^S$  basically have similar strengths and the same signs, positive at  $y > 0$  and negative at  $y < 0$ . For the electrons along  $+x$  direction, the magnetic force is opposite to the electric force, which can result in electron wiggling along the  $y$  direction with the force  $-e(E_y^S - v_{e,x}B_z^S)$ . With  $v_{e,x} \simeq 1$ , the wiggler field around the surfaces  $y \simeq \pm 0.3\mu m$  can be written by

$$F_y^{wiggler} \simeq E_y^S - B_z^S. \quad (1)$$

Note that contributions of laser electric and magnetic fields to  $F_y^{wiggler}$  (and resulting  $\chi$  [43]) are counteracted. One can write  $F_z^{wiggler} \simeq E_z^S + B_y^S$  around the surfaces  $z \simeq \pm 0.3\mu m$ .

Now we analyze if  $F_y^{wiggler}$  can lead to effective wiggling motion. Formation of the electrostatic and magnetostatic fields can be described by  $\partial E_y^S/\partial y + \partial E_z^S/\partial z = 2\pi(n_i - n_e)$  and  $\partial B_z^S/\partial y - \partial B_y^S/\partial z = 2\pi J_x$ , where  $E_x^S$ ,  $B_x^S$ , static  $J_y$  and  $J_z$  are relatively weak as observed in

our PIC simulation. Here  $n_i$  and  $n_e$  are normalized by  $n_c$ ,  $J_x$  by  $ecn_c$ , and fields by  $m_e c \omega_0 / e$ . According to our PIC simulation, we find that  $E_z^S$ ,  $B_y^S$ ,  $\partial E_z^S / \partial z$ , and  $\partial B_y^S / \partial z$  are roughly constant at the surface with a given  $z$  since the wire width are much smaller than the laser spot diameter [one can similarly see in Figs. 2(a) and 2(c) that  $E_y^S$ ,  $B_z^S$ ,  $\partial E_y^S / \partial y$  and  $\partial B_z^S / \partial y$  are roughly constant at the surface with a given  $y$ ]. Then,  $\partial E_y^S / \partial y \simeq 2\pi(n_i - n_e - \alpha_1)$  and  $\partial B_z^S / \partial y = 2\pi(J_x - \alpha_2)$  at a given  $z_0$ , where  $\partial E_z^S / \partial z|_{z_0} \simeq 2\pi\alpha_1$  and  $-\partial B_y^S / \partial z|_{z_0} = 2\pi\alpha_2$ . One can obtain:

$$\partial F_y^{wiggler} / \partial y \simeq 2\pi(n_i - n_e - J_x - \alpha_1 + \alpha_2) = 2\pi\rho^{eff}. \quad (2)$$

According to this equation, one can understand Figs. 2(e) and 2(f), where we simply take  $\alpha_1 = 40$  and  $\alpha_2 = 30$  to satisfy neutrality at  $y = 0$ . Note that basically  $|\alpha_1 - \alpha_2|$  is far smaller than  $|n_i - n_e|$  and  $|J_x|$ , so that the effective charge density  $\rho^{eff}$  is mainly determined by  $n_i - n_e - J_x$ . Around the wire center,  $\rho^{eff} \simeq 0$ ; Increasing  $|y|$ , electrons are piled up by laser radiation pressure with  $n_e > n_i$  and return currents are mainly located this region with  $J_x > 0$ , and consequently  $\rho^{eff} < 0$ ; Further increasing  $|y|$  and close to the surface, wire electrons are stripped with  $n_e \sim 0$ , there are well-guided beams in the ion channel with  $J_x < 0$ , and thus  $\rho^{eff} \simeq n_i - J_x > 0$  [see Fig. 2(f)].

Such  $\rho^{eff}$  generates effective wiggler fields  $F_y^{wiggler}$  shown in Fig. 2(e). There are two zero-field points close to the surfaces  $y \simeq \pm 0.3\mu m$ , respectively. Around these points the fields are bipolar, which naturally causes electron wiggler. Note that the peak field strength inside the wire is higher than that outside, which prevents the beam electrons from crossing the wire center and keeps them wiggling at one side of the wire [see Fig. 3(a)]. One can also see in Fig. 2(e) that change of  $F_y^{wiggler}$  with  $y$  is sharp at the zero-field points due to large  $\rho^{eff} \simeq n_i$ . This causes small spatial displacement of the electron wiggling motion and small angles of photon emission [see Figs. 3(a) and 3(c)].

The trajectory and energy evolution for a test electron located around the wire surface  $y \simeq -0.3\mu m$  are plotted in Figs. 3(a) and 3(c). One can see in Fig. 3(a) that the field  $E_y - B_z$  experienced by the electron varies with the transverse position  $y$  but not with  $x$  since it moves along with the laser at  $v_{e,x} \simeq 1$ . This suggests that its wiggling motion is driven by the static fields rather than the laser fields. As the pulse moves to the focusing plane  $x = 25\mu m$ , the electron energy  $\varepsilon$  grows gradually to  $>1\text{GeV}$  with increasing QED parameter  $\chi$  and decreasing emission angles  $\theta$ . Around the focusing plane, the strongest

emission arises with the largest  $\chi \simeq 0.2$  accompanied with the smallest  $\theta \simeq 1^\circ$  and therefore the  $\gamma$ -rays have the angle peak around  $1^\circ$  [see Figs. 1(d) and 4(a)]. At later, both  $\varepsilon$  and  $\chi$  decrease while  $\theta$  increases. This is why we take the laser focusing plane a few Rayleigh lengths behind the wire fore-end, allowing a distance to accelerate and generate well-guided GeV beam before the highest laser intensity and resulting the largest  $\chi$ . The QED parameter  $\chi = \gamma_e \sqrt{(\mathbf{E} + \mathbf{v}_e \times \mathbf{B})^2 - (\mathbf{v}_e \cdot \mathbf{E})^2} / E_{Sch}$  [40–42] of an electron with  $v_{e,x} \simeq 1$  can be simplified as

$$\chi \simeq \gamma_e |E_y^S - B_z^S| / E_{Sch}, \quad (3)$$

for the wiggler along the y direction, where  $E_{Sch} = 1.32 \times 10^{18} \text{V/m}$  is the Schwinger strength [44, 45], and  $\gamma_e$  and  $\mathbf{v}_e$  are electron relativistic factor and velocity normalized by  $c$ . According to Eq. (3) with  $|E_y^S - B_z^S| \simeq 50$ ,  $\gamma_e \simeq 1957$  read from Figs. 3(a) and 3(c), one can calculate  $\chi = 0.23$  in agreement with Fig. 3(c).

Figure 4 indicates that our scheme is robust. Similar photon angular distributions are achieved when the power is ranging from 0.5PW to 5PW available currently [19, 21] and the width from  $0.5\mu\text{m}$  and  $0.8\mu\text{m}$  (even with similar conversion efficiencies). In particular, even at 0.5PW the  $\gamma$ -ray brilliance can reach  $1.2 \times 10^{26} \text{ photons s}^{-1} \text{ mrad}^{-2} \text{ mm}^{-2} \text{ 0.1\% BW at 6MeV}$ . When the width is too small, e.g.,  $0.1\mu\text{m}$ , the wire is completely destroyed by the laser fields and electrons move like in the vacuum. Hence, the  $\gamma$ -rays have high divergence and low conversion efficiency. When increasing the width to  $0.3\mu\text{m}$ , the wire structure can be kept before the pulse approaches its focusing plane. Then, electrons are first wiggled around the wire surface and later cross the wire center with large angles when strongest radiation occurs due to  $\varepsilon$  and  $\chi$  at the maximums [see Figs. 3(b) and 3(d)]. This causes the  $\gamma$ -rays peaked at a larger angle than the  $0.6\mu\text{m}$  wire case [see Fig. 4(a)]. These can be seen more clearly in Figs. 3(e)-3(h) which show spatial, angular, energy distributions of electrons. In the  $0.6\mu\text{m}$  case [Figs. 3(e) and 3(g)], the higher-energy electrons are distributed around the surface and peaked at  $1^\circ$ , which have nC charge. They are wiggled on one side of the surface and then strongly emit  $\gamma$ -rays around  $1^\circ$ . In the  $0.3\mu\text{m}$  case [Figs. 3(f) and 3(h)], however, the electrons are peaked at the wire center and around  $10^\circ$ , where the pulse is absorbed more strongly since it can enter the wire interior, rather than being stopped by the surface in the  $0.6\mu\text{m}$  wire. Thus, the conversion efficiency appears highest around  $0.3\mu\text{m}$  [see Fig. 4(c)]. For the same reason, the efficiency decreases with the increasing wire width.

To further understand Figs. 4(d) and 4(e), we analyze the photon energy and number scaling with the laser power. The electron beam energy can be given by  $\langle\gamma_e\rangle \simeq 3.13a_0 \exp(-\lambda_0^2/16r_0^2)$  according to Ref. [31], which predicts the value 437MeV close to the peak energy 650MeV shown in Fig. 3(g). Then, Eq. (3) can be rewritten by  $\langle\chi\rangle \simeq 3.13a_0 \exp(-\lambda_0^2/16r_0^2)|F_y^{wiggler}|/E_{Sch}$ . In our case with the peak intensity around  $10^{23}$  Wcm $^{-2}$  and the wire width below  $\lambda_0$ , the electrons on the wire surface are quickly stripped and therefore, the static field strength or  $|F_y^{wiggler}|$  depends strongly upon the wire charge density and weakly upon the laser intensity, as observed in our simulations and Eq. (2). When the wire parameter is fixed and the laser power  $P_0$  is adopted within 0.5 to 5PW, one can roughly take  $|F_y^{wiggler}|$  as a value about 50 according to our simulations and then  $\langle\chi\rangle \simeq 0.00037a_0$ . To obtain photon data, one can use the theory of synchrotron radiation [32, 43], which is general when the acceleration field of an electron is given in its rest frame, i.e.,  $\chi$ . The emitted photons have an average energy

$$\langle\varepsilon_{ph}\rangle = 0.44\langle\chi\rangle\langle\gamma_e\rangle m_e c^2 \simeq 0.000245a_0^2 \text{ [MeV]} \quad (4)$$

and the photon generation rate per electron is  $1.4 \times 10^{13}\langle\gamma_e\rangle \simeq 4.2 \times 10^{13}a_0$ . With  $P_0 = 5, 2.5, 1, 0.5$ PW,  $\langle\varepsilon_{ph}\rangle$  is calculated as 40, 20, 8, 4MeV, respectively, which reasonably agrees with our simulation results: 31, 20, 13, 6MeV. To obtain the photon number, we count the number  $N_e$  of electrons above 10MeV in our simulations and find a rough scaling  $Ne \propto a_0^2$ . We assume that beam electrons have nearly the same efficient radiation time with  $P_0$  ranging from 0.5PW to 5PW, since the pulse spot size is much larger than the wire width and therefore the wire slightly affects the evolution of the pulses with different  $P_0$ . Then, the photon number follows

$$N_{ph} \propto a_0^3, \quad (5)$$

which agrees with our simulation results:  $2.8 \times 10^{12}, 1.24 \times 10^{12}, 3.6 \times 10^{11}$ , and  $1.6 \times 10^{11}$  photons with 5, 2.5, 1, and 0.5 PW, respectively. From Eqs. (4) and (5), one can obtain the conversion efficiency  $\eta \propto a_0^3$ , in reasonable agreement with the results shown in Fig. 4(d).

In summary, we have shown that a PW-laser-irradiated sub-wavelength solid wire acts as a novel wiggler and an accelerator of nC, GeV, high-directivity electron beams. The wiggler is driven by electrostatic and magnetostatic fields around the wire surface, rather than directly by the laser fields. Due to high density of the wire, the quasistatic fields are



so high that the wiggling electrons have  $\chi > 0.1$ . With the synchrotron radiation in the QED regime, ultra-bright, tens-of-MeV, few-mrad-divergence  $\gamma$ -rays peaked at  $1^\circ$  can be efficiently generated with  $P_0$  between 0.5PW and 5PW. The average photon energy scales linearly with  $P_0$  and the photon number and conversion efficiency with  $P_0^{3/2}$ . In our scheme, the laser focusing plane should be behind the wire fore-end, allowing a distance to generate well-guided GeV beams before achieving the largest  $\chi$ .

This work was supported by Science Challenge Project of China (Grant No. TZ2016005), the National Basic Research Program of China (Grants No. 2013CBA01500), the National Natural Science Foundation of China (Grants No. 11775302, No. 11375261, No.11421064, No. 11374210, No. 113111048, and No.11520101003), and the Strategic Priority Research Program of the Chinese Academy of Sciences (Grants No. XDB16010200 and No.XDB07030300). Z.M.S. acknowledges the support of a Leverhulme Trust Research Grant and EPSRC (UK) Grant No. EP/N028694/1, and EC's H2020 EuPRAXIA (Grant No. 653782).

- 
- [1] S. V. Bulanov, T. Zh. Esirkepov, M. Kando, J. Koga, K. Kondo, and G. Korn, *Plasma Phys. Rep.* **41**, 1 (2015).
  - [2] D. Habs, M.M. Guenther, M. Jentschel, P.G. Thirolf, *Nuclear Photonics* (<https://arxiv.org/abs/1201.4466>)
  - [3] C. Barty, *Nuclear Photonics for the 21st Century*, Optics and Photonics International Congress, April 22-25, 2015, Yokohama, Japan.
  - [4] T. S. Lawrence, R. K. Ten Haken, and A. Giaccia, *Principles of Radiation Oncology*, 8th ed. (Lippincott, Williams, and Wilkins, Philadelphia, 2008).
  - [5] K. J. Weeks, V. N. Litvinenko, and J. M. J. Madey, *Med. Phys.* **24**, 417 (1997).
  - [6] T. Tajima and J. M. Dawson, *Phys. Rev. Lett.* **43**, 267 (1979).
  - [7] E. Esarey, C. B. Schroeder, and W. P. Leemans, *Rev. Mod. Phys.* **81**, 1229 (2009).
  - [8] A. Rousse, K. T. Phuoc, R. Shah, A. Pukhov, E. Lefebvre, V. Malka, S. Kiselev, F. Burgy, J.-P. Rousseau, D. Umstadter, and D. Hulin, *Phys. Rev. Lett.* **93**, 135005 (2004).
  - [9] S. Kneip, C. McGuffey, J. L. Martins, S. F. Martins, C. Bellei, V. Chvykov, F. Dollar, R. Fonseca, C. Huntington, G. Kalintchenko, A. Maksimchuk, S. P. D. Mangles, T. Matsuoka,

- S. R. Nagel, C. A. J. Palmer, J. Schreiber, K. Ta Phuoc, A. G. R. Thomas, V. Yanovsky, L. O. Silva, K. Krushelnick and Z. Najmudin, *Nat. Phys.* **6**, 980 (2010).
- [10] S. Cipiccia, M. R. Islam, B. Ersfeld, R. P. Shanks, E. Brunetti, G. Vieux, X. Yang, R. C. Issac, S. M. Wiggins, G. H. Welsh, M.-P. Anania, D. Maneuski, R. Montgomery, G. Smith, M. Hoek, D. J. Hamilton, N. R. C. Lemos, D. Symes, P. P. Rajeev, V. O. Shea, J. M. Dias and D. A. Jaroszynski, *Nat. Phys.* **7**, 867 (2011).
- [11] K. Ta Phuoc, S. Corde, C. Thauray, V. Malka, A. Tafzi, J. P. Goddet, R. C. Shah, S. Sebban, and A. Rousse, *Nat. Photonics* **6**, 308 (2012).
- [12] S. Chen, N. D. Powers, I. Ghebregziabher, C. M. Maharjan, C. Liu, G. Golovin, S. Banerjee, J. Zhang, N. Cunningham, A. Moorti, S. Clarke, S. Pozzi, and D. P. Umstadter, *Phys. Rev. Lett.* **110**, 155003 (2013).
- [13] N. D. Powers, I. Ghebregziabher, G. Golovin, C. Liu, S. Chen, S. Banerjee, J. Zhang, and D. P. Umstadter, *Nat. Photonics* **8**, 28 (2014).
- [14] C. Liu, G. Golovin, S. Chen, J. Zhang, B. Zhao, D. Haden, S. Banerjee, J. Silano, H. Karwowski, and D. Umstadter, *Opt. Lett.* **39**, 4132 (2014).
- [15] G. Sarri, D. J. Corvan, W. Schumaker, J. M. Cole, A. Di Piazza, H. Ahmed, C. Harvey, C. H. Keitel, K. Krushelnick, S. P. D. Mangles, Z. Najmudin, D. Symes, A. G. R. Thomas, M. Yeung, Z. Zhao, and M. Zepf, *Phys. Rev. Lett.* **113**, 224801 (2014).
- [16] K. Khrennikov, J. Wenz, A. Buck, J. Xu, M. Heigoldt, L. Veisz, and S. Karsch, *Phys. Rev. Lett.* **114**, 195003 (2015).
- [17] C. You et al., *Sci. Rep.* **6**, 29518 (2016).
- [18] W. Yan, C. Fruhling, G. Golovin, D. Haden, J. Luo, P. Zhang, B. Zhao, J. Zhang, C. Liu, M. Chen, S. Chen, S. Banerjee and D. Umstadter, *Nat. Photonics* **11**, 514 (2017).
- [19] <https://apri.gist.ac.kr/en/page/menu02/page0101.php>
- [20] I. J. Kim, K. H. Pae, I. W. Choi, C.-L. Lee, H. T. Kim, H. Singhal, J. H. Sung, S. K. Lee, H. W. Lee, P. V. Nickles, T. M. Jeong, C. M. Kim, and C. H. Nam, *Phys. Plasma* **23**, 070701 (2016).
- [21] [http://www.cst.sh.cn/yw2016/201609/t20160912\\_4660822.html](http://www.cst.sh.cn/yw2016/201609/t20160912_4660822.html)
- [22] J. Fischer and M. Wegener, *Laser Photonics Rev.* **7**, 22 (2013).
- [23] [https://www.xfel.eu/facility/comparison/index\\_eng.html](https://www.xfel.eu/facility/comparison/index_eng.html)
- [24] <http://www.esrf.eu/home/UsersAndScience/Accelerators.html>

- [25] [http://e-ssrf.sinap.cas.cn/beamlines/bl115u1/201401/t20140112\\_152434.html](http://e-ssrf.sinap.cas.cn/beamlines/bl115u1/201401/t20140112_152434.html)
- [26] R. Hettel, *Short Pulse Laser Interactions with Matter*, 8th ICFA Advanced Beam Dynamics Workshop on Future Light Sources (2010).
- [27] R. Kodama, Y. Sentoku, Z. L. Chen, G. R. Kumar, S. P. Hatchett, Y. Toyama, T. E. Cowan, R. R. Freeman, J. Fuchs, Y. Izawa, M. H. Key, Y. Kitagawa, K. Kondo, T. Matsuoka, H. Nakamura, M. Nakatsutsumi, P. A. Norreys, T. Norimatsu, R. A. Snavely, R. B. Stephens, M. Tambo, K. A. Tanaka, and T. Yabuuchi, *Nature* **432**,1005 (2004).
- [28] S. Tokita, K. Otani, T. Nishoji, S. Inoue, M. Hashida, and S. Sakabe, *Phys. Rev. Lett.* **106**, 255001 (2011).
- [29] H. Nakajima, S. Tokita, S. Inoue, M. Hashida, and S. Sakabe, *Phys. Rev. Lett.* **110**, 155001 (2013).
- [30] Y. T. Li, X. H. Yuan, M. H. Xu, Z. Y. Zheng, Z. M. Sheng, M. Chen, Y. Y. Ma, W. X. Liang, Q. Z. Yu, Y. Zhang, F. Liu, Z. H. Wang, Z. Y. Wei, W. Zhao, Z. Jin, and J. Zhang, *Phys. Rev. Lett.* **96**, 165003 (2006).
- [31] Y.-Y. Ma, Z.-M. Sheng, Y.-T. Li, W.-W. Chang, X.-H. Yuan, M. Chen, H.-C. Wu, J. Zheng, and J. Zhang, *Phys. Plasmas* **13**, 110702 (2006).
- [32] C. P. Ridgers, C. S. Brady, R. Duclous, J. G. Kirk, K. Bennett, T. D. Arber, A. P. L. Robinson, and A. R. Bell, *Phys. Rev. Lett.* **108**, 165006 (2012).
- [33] C. S. Brady, C. P. Ridgers, T. D. Arber, A. R. Bell, and J. G. Kirk, *Phys. Rev. Lett.* **109**, 245006 (2012).
- [34] W.-M. Wang, P. Gibbon, Z.-M. Sheng, Y.-T. Li, and J. Zhang, *Phys. Rev. E* **96**, 013201 (2017).
- [35] H. X. Chang et al., *Sci. Rep.* **7**, 45031 (2017).
- [36] D. J. Stark, T. Toncian, and A. V. Arefiev, *Phys. Rev. Lett.* **116**, 185003 (2016).
- [37] W.-M. Wang, P. Gibbon, Z.-M. Sheng, and Y.-T. Li, *Phys. Rev. E* **91**, 013101 (2015).
- [38] W.-M. Wang, Z.-M. Sheng, P. Gibbon, and Y.-T. Li, *Modeling of photon and pair generation due to quantum electrodynamics effects in particle-in-cell simulation* (<http://arxiv.org/abs/1608.06356>).
- [39] P. Gibbon, *Short Pulse Laser Interactions with Matter* (Imperial College Press, London, 2000).
- [40] T. Erber, *Rev. Mod. Phys.* **38**, 626 (1966).
- [41] N. V. Elkina, A. M. Fedotov, I. Yu. Kostyukov, M. V. Legkov, N. B. Narozhny, E. N. Nerush,

- and H. Ruhl, Phys. Rev. ST Accel. Beams **14**, 054401 (2011).
- [42] A. Di Piazza, C. Muller, K. Z. Hatsagortsyan, and C. H. Keitel, Rev. Mod. Phys. **84**, 1177 (2012).
- [43] A. R. Bell and J. G. Kirk, Phys. Rev. Lett. **101**, 200403 (2008).
- [44] F. Sauter, Z. Phys. **69**, 742 (1931).
- [45] J. Schwinger, Phys. Rev. **82**, 664 (1951).

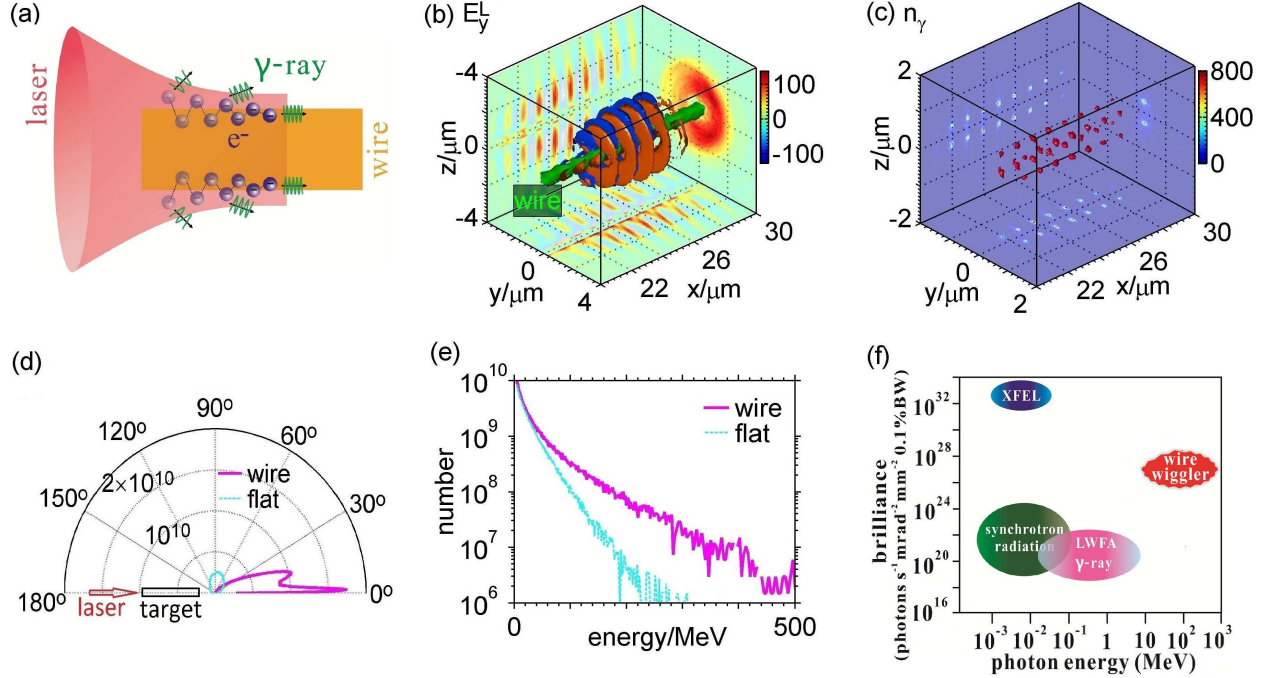


FIG. 1. (a) Schematic: as a laser propagates along a subwavelength wire and approaches its focusing plane, electrons along the wire surface are gradually accelerated with reduced divergent angles, meanwhile, the electrons are wiggled perpendicularly to the surface, which causes  $\gamma$ -rays emitted with increased photon energies and decreased divergent angles. Three-dimensional isosurfaces of (b) the laser field (units of  $m c \omega_0 / e$ ) and (c)  $\gamma$ -ray photon density (units of  $n_c$ ) at the time of  $30\tau_0$  as well as the slices at the planes with respective peak values, where a  $0.6\mu\text{m}$ -wide wire is taken. (d) Angular distributions and (e) spectra of  $\gamma$ -rays emitted from the wire and a flat target, respectively. (f) Photon energy and brilliance of  $\gamma$ -rays generated from synchrotron radiation facilities, XFEL [23], betatron radiation and Compton scattering based on LWFA, and our scheme.

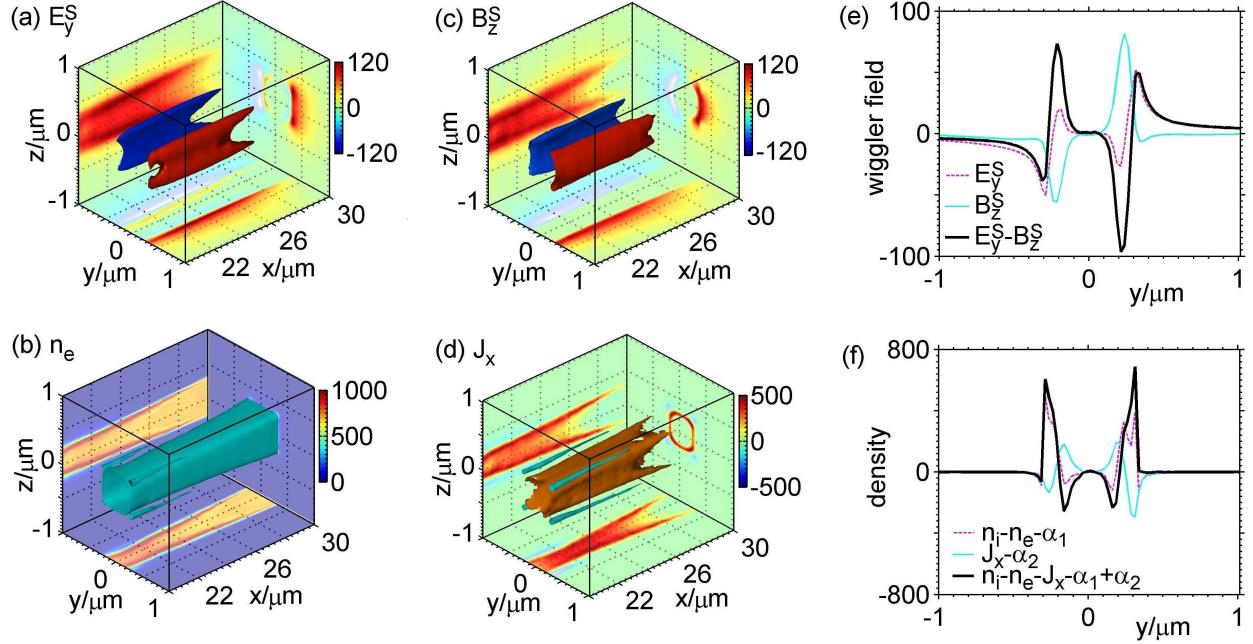


FIG. 2. Three-dimensional isosurfaces of (a) electrostatic and (c) magnetostatic fields (units of  $mc\omega_0/e$ ), (b) electron density (units of  $n_c$ ), and (d) current density (units of  $ecn_c$ ) at the time of  $30\tau_0$  as well as the slices at the planes with respective peak values, where they are obtained by temporally averaging  $E_y$ ,  $B_z$ ,  $n_e$ , and  $J_x$ , respectively, over one laser cycle. The corresponding one-dimensional distributions of these fields and densities at  $x = 21\mu\text{m}$  and  $z = 0.26\mu\text{m}$  are shown in (e) and (f).

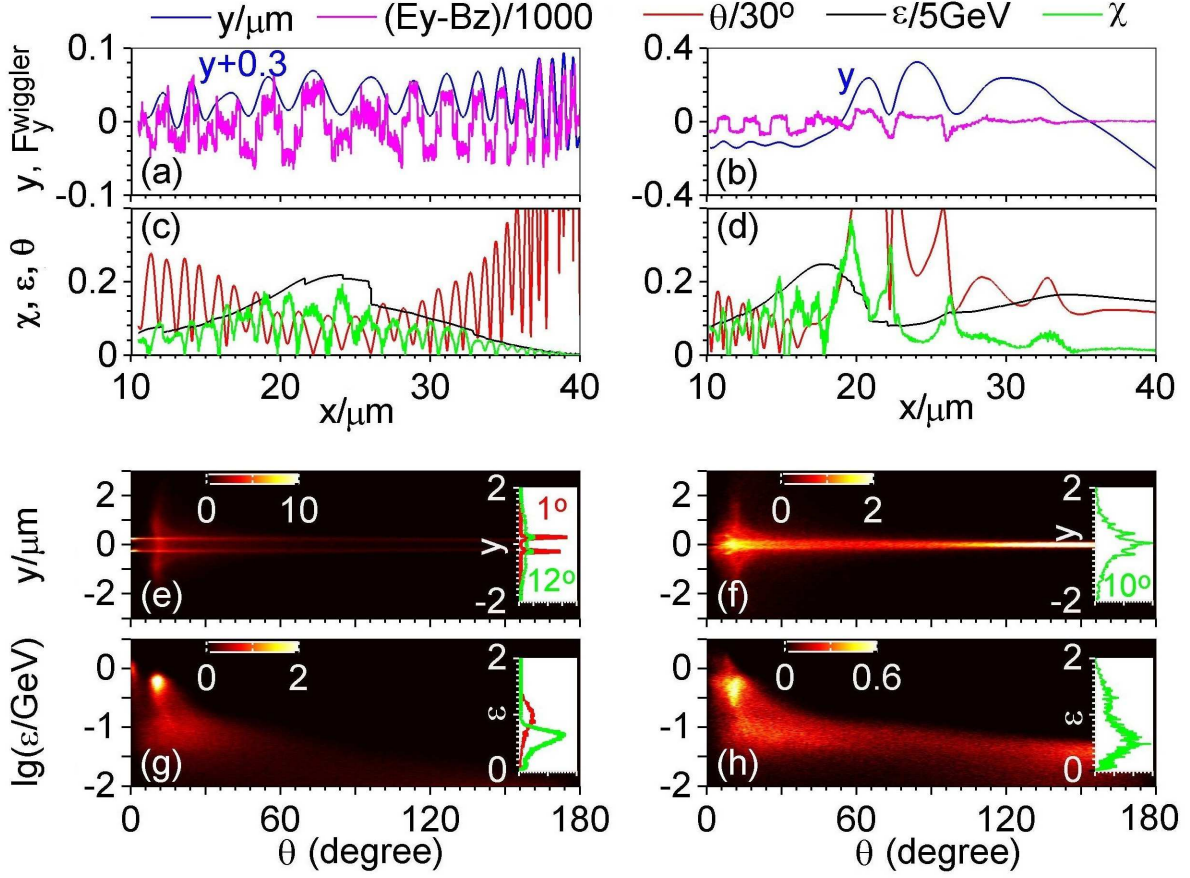


FIG. 3. Evolution for a test electron from the  $0.6\mu m$  [(a), (c)] and  $0.3\mu m$  wires [(b), (d)], respectively, is shown of the transverse position  $y$  (units of  $\mu m$ ), divergence angle  $\theta$  (units of  $30^\circ$ ), energy  $\varepsilon$  (units of  $5\text{GeV}$ ), QED parameter  $\chi$ , and  $E_y - B_z$  (units of  $1000m_e c\omega_0/e$ ), where we plot  $y+0.3$  in (a) since the electron wiggles around  $-0.3\mu m$ . (e)-(h) Number (units of  $10^8$ ) of electrons  $>10\text{MeV}$  as a function of  $(\theta, y, \varepsilon)$  at  $30\tau_0$ , where insets in each plot show number distributions at given angles. The left and right columns correspond to  $0.6\mu m$  and  $0.3\mu m$  wires, respectively.



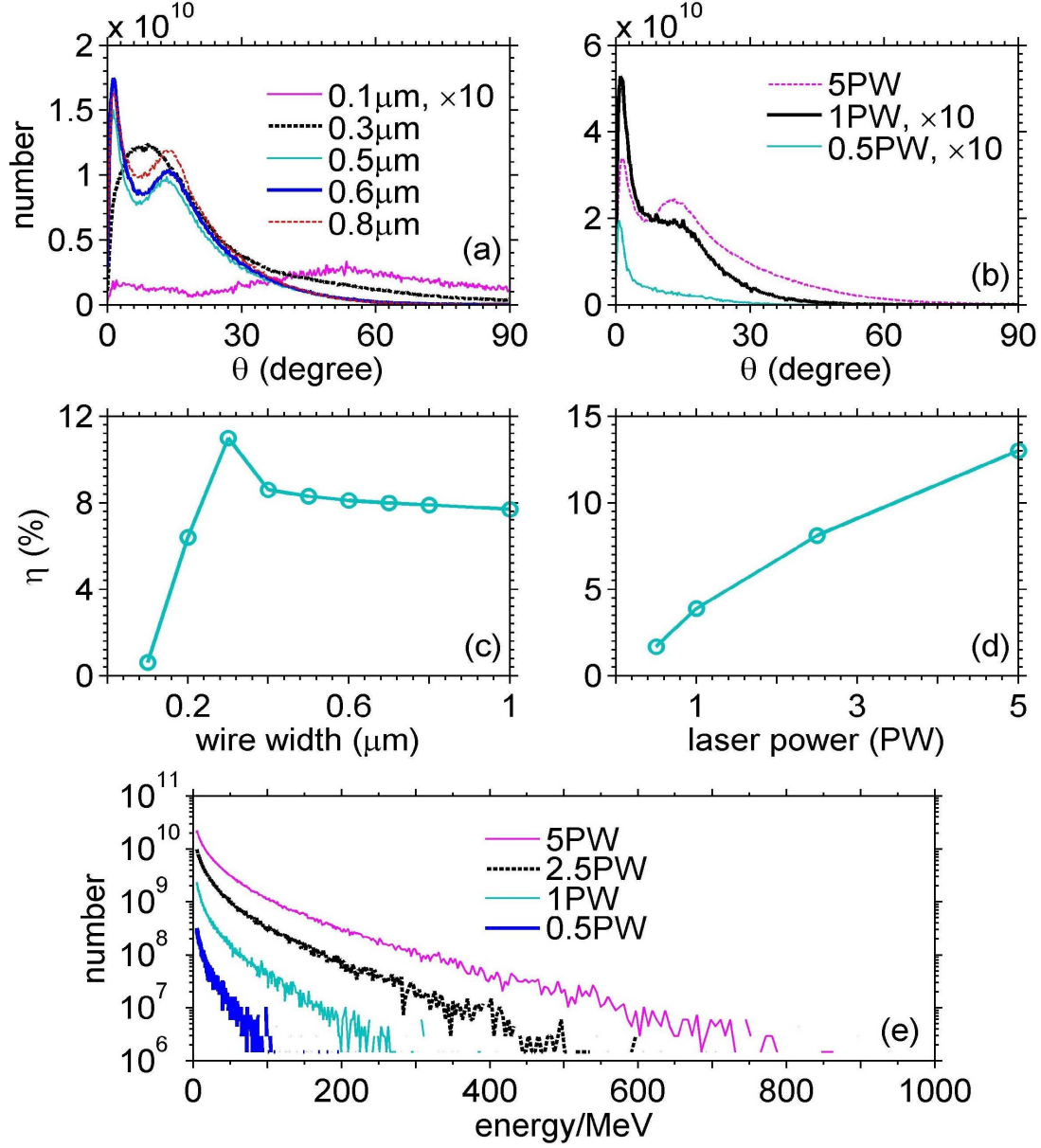


FIG. 4. Angular distributions of  $\gamma$ -rays with different wire widths (a) and laser powers (b), where “ $\times 10$ ” in the legend means the number multiplied by 10.  $\gamma$ -ray conversion efficiency versus (c) wire widths and (d) laser powers. (e)  $\gamma$ -ray spectra at  $50\tau_0$  under different powers. In (a) and (c), the power is fixed at 2.5PW. In (b), (d), and (e), the wire width is fixed at  $0.6\mu\text{m}$ .